Journal of Electronic Research and Application, 2026, Volume 10, Issue 4
http://ojs.bbwpublisher.com/index.php/JERA
Online ISSN: 2208-3510
Print ISSN: 2208-3502

Simulation Study on Corrosion Behavior of High Entropy Oxide Modified Epoxy Coating

Zhongli Dong[1], Chao Wang[2]*, Ming Nie[1]

[1]Electric Power Research Institute of Guangdong Power Grid Co., Ltd., Guangzhou 510080, Guangdong, China
[2]Wuhan University of Technology, Wuhan 430070, Hubei, China

Corresponding author: Chao Wang, wchao@whut.edu.cn

Abstract: The widespread application of aluminum alloys in automotive lightweighting is frequently compromised by corrosion initiated at coating defects, yet the specific failure mechanisms governed by defect morphology remain difficult to isolate via traditional experimentation. This study employs a two-dimensional multiphysics coupling model, constructed on the COMSOL platform, to quantitatively investigate the corrosion evolution of epoxy-coated aluminum alloys containing two representative defect types: interfacial delamination and through-thickness bubbles. By integrating electrochemical kinetic parameters, the simulation elucidates how defect geometry modulates potential fields, current density distributions, and ionic transport within the "coating–electrolyte–substrate" system. Results indicate that delamination thickness positively correlates with corrosion rates; thicker cavities (50μm) significantly reduce ohmic resistance, thereby accelerating micro-galvanic coupling between the α-Al matrix and β-phase and expanding the corrosion domain. Furthermore, a distinct size effect was observed for through-thickness bubbles: large-scale defects (50μm) facilitate unimpeded mass transport, leading to severe lateral propagation and extensive substrate loss due to stable charge loops. Conversely, small-scale defects (20μm) induce a pronounced occluded cell effect, generating high local current densities that drive rapid vertical penetration, identifying them as the critical factor for deep-base pitting. These findings provide a theoretical basis for optimizing coating integrity and predicting localized corrosion behaviors in aluminum alloy structures.

Keywords: Aluminum alloys; Epoxy resin; High-entropy oxides; Numerical simulation; Coating

Online publication: May 21, 2026

1. Introduction

With the advancement of automotive lightweighting, aluminum alloys have been extensively applied in critical body structures, bringing corrosion issues to the forefront [1]. Although organic coatings serve as the primary protection strategy due to their superior barrier properties, manufacturing constraints and substrate conditions inevitably induce defects such as pores, micro-cracks, and interfacial debonding. These

imperfections significantly compromise the actual protective efficacy compared to design expectations [2,3].

Given the inherent limitations of traditional experimental methodologies, characterized by protracted cycles, high costs, and complexities in variable control, this study employs numerical simulation techniques based on the COMSOL Multiphysics platform to construct a corrosion model for defective epoxy coating-aluminum alloy systems. By integrating experimentally derived electrochemical kinetic parameters under established physical assumptions, this research elucidates the multi-field coupling mechanisms through which defect characteristics (size, distribution, and type) govern the substrate's potential field, current density distribution, ionic concentration profiles, and interfacial reaction rates [4,5]. Consequently, this work quantitatively evaluates the localized corrosion behavior of defective coatings, providing a robust theoretical foundation and design guidelines for the precise control of coating defects and the optimization of protective performance.

2. Simulation model

To balance computational efficiency with simulation fidelity, this study constructs a two-dimensional cross-sectional model to approximate the three-dimensional corrosion behavior of the defective epoxy coating/aluminum alloy system. The computational domain comprises three distinct regions: the electrolyte (3.5wt% NaCl solution), the coating layer, and the aluminum alloy substrate. Two representative defect morphologies are investigated: (a) delamination defects, modeled with a substrate thickness of 100μm and width of 200μm, featuring interfacial gap heights of 20μm and 50μm; and (b) through-thickness bubble defects, characterized by a 100μm thick coating containing vertical channels with widths of 20μm and 50μm, situated above a substrate of identical dimensions (100μm thickness, 200μm width).

The corrosion evolution of the aluminum alloy is governed primarily by anodic dissolution kinetics and charge transfer mechanisms at the electrolyte-metal interface. Given the pronounced potential gradients and current density concentrations inherent to defective regions, an extremely fine mesh discretization was implemented within the substrate domain, with localized refinement applied to the immediate vicinity of the substrate-electrolyte interface. This strategy ensures the precise capture of steep electrochemical field variations and guarantees numerical convergence. The specific mesh discretization scheme is illustrated in **Figure 1**.

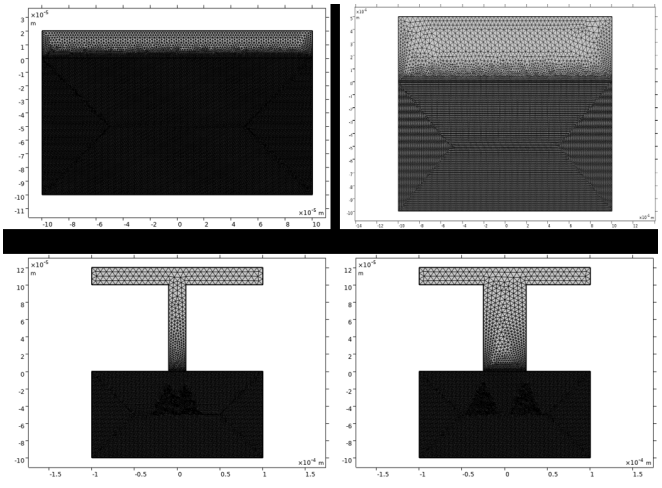

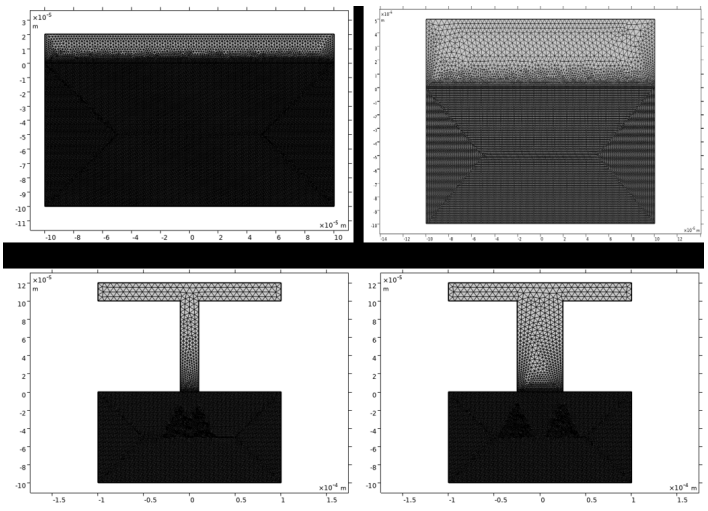

Figure 1. Mesh discretization of the aluminum alloy corrosion model featuring bubble defects.

3. Influence of different defects on the electrolyte potential of aluminum alloys

3.1. Influence of delamination defects on the electrolyte potential of aluminum alloys

Figure 2 illustrates the spatiotemporal evolution characteristics of the electrolyte potential within aluminum alloy systems containing delamination defects. In terms of spatial distribution, the substrate regions distant from the β-phase exhibit relatively higher potentials, whereas areas adjacent to the β-phase show significantly reduced potentials, characterized by abrupt potential gradients at the two-phase interface. This phenomenon is attributed to the micro-galvanic corrosion mechanism: the α-Al matrix acts as the anode undergoing dissolution (corresponding to higher potentials), while the Cu-rich β-phase serves as the cathode facilitating the oxygen reduction reaction (corresponding to lower potentials), with the electrolyte trapped within the delamination cavities constituting the ionic conduction loop. Furthermore, the counter-flow of ions-specifically, the migration of anodically generated Al^{3+} towards the cathode and the diffusion of cathodically generated OH^- towards the anode-further exacerbates potential distortion in the interfacial vicinity.

Regarding temporal evolution, at 150h, the potential field displays a continuous gradient distribution; notably, the 50μm delamination case exhibits a smoother color transition, indicating that the thicker cavity reduces the equivalent ohmic resistance and establishes a more stable charge transport pathway. By 450 h, the potential field in the 50μm delamination scenario has evolved into a high-potential state covering the entire corrosion interface, signaling that the system has entered a stage of comprehensive, sustained corrosion, whereas the 20μm case remains lagging behind this advanced evolutionary stage.

The increase in delamination thickness significantly enhances the potential gradient and the reaction sustainability by reducing the equivalent resistance of the electrolyte pathway, thereby expanding the domain of corrosion influence; concurrently, the interface potential abruptness induced by the β-phase further accelerates the kinetics of the micro-galvanic corrosion process.

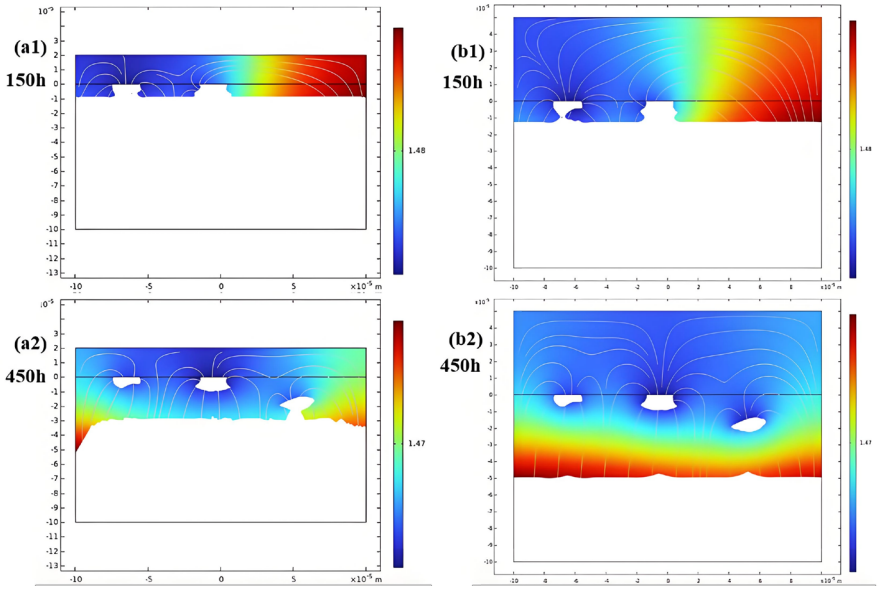

Figure 2. Variation of electrolyte potential with time: (a) 20μm delamination; (b) 50μm delamination.

3.2. Influence of delamination defects on the electrolyte potential of aluminum alloys

Figure 3 illustrates the spatiotemporal evolution characteristics of the electrolyte potential in aluminum alloy systems featuring through-thickness bubble defects of varying sizes. The results demonstrate that bubble size significantly modulates the degree of potential field distortion and its spatial distribution, inducing current line convergence and abrupt potential gradients under the synergistic effect of the β-phase.

At 150 h, the electrolyte penetrates the substrate directly through the through-channels, with initial potential disturbances emerging at the defect openings and regions adjacent to the β-phase. Compared to the 20μm case, the 50μm defect exhibits more severe bending of equipotential lines and a broader disturbance range, indicating that larger channels effectively reduce equivalent ohmic resistance and mass transfer impedance, thereby accelerating the establishment of stable electrochemical gradients and the formation of charge transport loops. By 450 h, as corrosion enters a stable propagation stage, the potential disturbance zone continues to expand; the 50μm case maintains an extensive region of strong gradients, signaling a severe failure of the coating's barrier function and sustained high-rate corrosion.

Correlating with the volume fraction analysis from the preceding section, although the lateral corrosion area for the 50μm defect is significantly larger, the vertical corrosion depths for both cases are comparable. The underlying mechanism is as follows: the 20μm defect, constrained by its narrow channel, readily induces a pronounced occluded cell effect, leading to highly concentrated local current densities that drive rapid vertical corrosion propagation (characteristic of pitting); conversely, the 50μm defect, benefiting from unimpeded mass transport, favors a corrosion morphology trending towards uniformity or lateral expansion.

In summary, large-scale (50μm) through-thickness bubble defects accelerate lateral propagation by reducing transport resistance and amplifying micro-galvanic effects, establishing strong potential gradients at an earlier stage. In contrast, small-scale (20μm) bubble defects, leveraging their advantage of high local current density, dominate vertical corrosion penetration, serving as the critical factor inducing deep-base pitting in aluminum alloys.

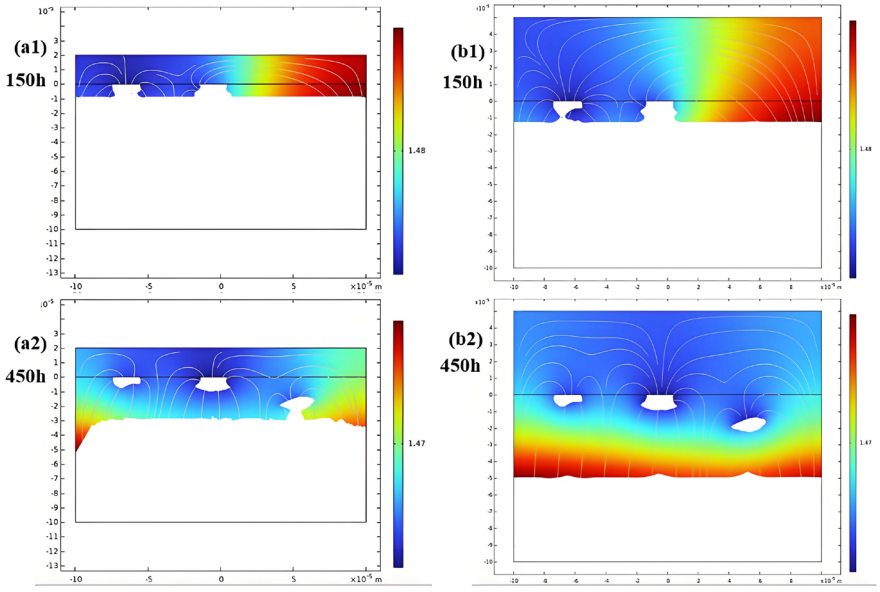

Figure 3. Variation of aluminum alloy volume fraction with time: (a) 20μm through-thickness bubble; (b) 50μm through-thickness bubble.

4. Conclusion

This study employed numerical simulations to investigate the failure mechanisms of epoxy-coated aluminum alloys containing defects. To overcome the experimental challenges associated with the independent manipulation of single variables, a two-dimensional multiphysics coupling model encompassing the "coating defect–electrolyte–aluminum alloy substrate" system was constructed. This framework facilitated a systematic exploration of the evolution characteristics of through-thickness bubble defects. The simulations revealed that through-thickness channels establish rapid pathways for electrolyte access to the substrate, inducing concentrated electrochemical reactions at the defect base and driving the lateral expansion of potential field distortions. Size effect analysis demonstrated distinct corrosion morphologies: large-scale bubbles, characterized by low mass transfer resistance and stable charge transport loops, exhibited more drastic variations in potential gradients and significant substrate loss, predominantly manifesting as lateral propagation. In contrast, small-scale bubbles, constrained by geometric limitations, fostered high local current densities, thereby dominating rapid vertical corrosion penetration. Consequently, small-scale bubbles are identified as the critical factor inducing deep-base pitting in aluminum alloys.

Funding

Science and Technology Project of China Southern Power Grid Co., Ltd. (Project No.: GDKJXM20222546)

Disclosure statement

The author declares no conflict of interest.

References

[1] Zhang T, Wang Y, Zhong S, Guidance Information Processing Methods in Aircraft Optical Imaging Seeker, National Defence Industry Press, Beijing.

[2] Yin X, Fei J, Aero-Optical Principles, China Aerospace Publishing House, Beijing.

[3] Chen C, Yi W, Cui W, 2018, Measurement of Infrared Radiation Characteristics of Space Targets Based on Reference Sources. Infrared and Laser Engineering, 47(8): 196–203.

[4] Li S, Liu Z, Liu K, et al., 2019, Research Progress in Aerospace Hyperspectral Remote Sensing Applications. Infrared and Laser Engineering, 48(3): 9–23.

[5] Huang Z, Li Y, Wang J, et al., 2022, Calibration of the EQUINOX 55 Remote Sensing Fourier Transform Infrared Spectroscopy System. Spectroscopy and Spectral Analysis, 22(3): 399–400.